

# Bone marrow absorption and retention properties of engineered scaffolds with micro-channels and nano-pores for tissue engineering: A proof of concept

Daniel S. Oh<sup>a,\*</sup>, Yoon Hyuk Kim<sup>b,\*\*</sup>, Danaa Ganbat<sup>b</sup>, Myung-Ho Han<sup>c</sup>,  
Phillip Lim<sup>a</sup>, Jung-Ho Back<sup>a</sup>, Francis Y. Lee<sup>a</sup>, Hesham Tawfeek<sup>a</sup>

<sup>a</sup>Department of Orthopedic Surgery, Center for Orthopedic Research, Columbia University, NY, USA

<sup>b</sup>Mechanical Engineering, Kyung Hee University, Yongin, Korea

<sup>c</sup>Department of Chemical Engineering, Kyungil University, Gyeongsan, Korea

Received 13 March 2013; received in revised form 5 April 2013; accepted 5 April 2013

Available online 25 April 2013

## Abstract

We have developed a hydroxyapatite-based scaffold with micro-channels and nano-pores (MCNP) using a polyurethane template coating method to overcome some of the limitations by addressing fluid absorbance and retention via capillary action. The novel scaffold has 3 basic structures. First, the scaffold has a porous trabecular network similar to that of human trabecular bones (300–400  $\mu\text{m}$ ) which are mechanically matched to the strength of native trabecular bone (2–12 MPa). Second, it has micro-sized channels (25–70  $\mu\text{m}$ ) within each trabecular septum which exhibit highly effective fluid absorption via capillary action. Third, the surface of each septum has nano-sized pores (100–400 nm) that allow immobilized cells to anchor. The surface area of the scaffold with micro-channels was significantly (+42.0%) higher than the scaffold without micro-channels as calculated using computer aided design (CAD) software, while overall porosity did not change significantly (+8.8%). Combinatorial effects of these internal structures result in a host-adapting construct that enhances cell ingress and retention from the host bone marrow throughout the entire scaffold.

© 2013 Elsevier Ltd and Techna Group S.r.l. All rights reserved.

**Keywords:** Tissue engineering; Microenvironment; Capillary action; Bone marrow ingress and retention

## 1. Introduction

The absence of a biologically functional environment in most grafts has hampered the potential for clinical applications and limited the success of bone tissue engineering [1–3]. To this day, successful grafting has hinged on the loading of pre-expanded mesenchymal stem cells (MSCs) and/or large amounts of growth factors, requiring elaborate laboratory techniques and excessive costs [4–6]. For this reason, inducing bone formation using natural environmental cues has become a major focus of tissue-engineering research. In the past decade,

scientists have employed a vast number of techniques to mimic natural bone characteristics such as pore size, porosity, inter-connectivity of the pores, and permeability in synthetic grafts [7–11]. These factors collectively play a role in cell attachment, proliferation, and differentiation as well as in nutrient flow and cell communication, all of which are crucial for proper bone healing [12,13]. Scientists continue to engineer characteristics of natural bone into grafts with the aims of simulating an environment highly suitable for normal bone processes such as cellular proliferation and osteogenic differentiation.

In addition to the structures themselves, many research groups have been developing scaffolds composed of different materials such as polymers, ceramics, metals, and even composite material. Extensive research has reaped relative success in terms of achieving some biocompatibility and mechanical strength. Designs include highly organized internal structures to provide cells with surfaces for attachment and

\*Corresponding author. Tel.: +1 212 305 7965; fax: +1 212 305 2741.

\*\*Corresponding author. Tel.: +82 31 201 2028; fax: +82 31 202 8106.

E-mail addresses: [dso2113@columbia.edu](mailto:dso2113@columbia.edu) (D.S. Oh),  
[yoohkim@khu.ac.kr](mailto:yoohkim@khu.ac.kr) (Y. Hyuk Kim).

<sup>1</sup>These two authors contributed equally to this work.

access to nutrients [14–16]. However, these highly organized structures are merely passive synthetic templates that have limited potential in overcoming the challenge of active initial cell infiltration upon graft insertion. These approaches have mostly resulted in the *in vitro* growth of tissue with cross-sections of less than a few millimeters from the external surface [17,18]. This is probably due to the diffusion constraints of the scaffold. Cells cannot migrate deep into the scaffold because of the lack of nutrients and oxygen while insufficiently removing waste products. Cell colonization at the scaffold-host bone junction may be acting as a physical barrier to the diffusion of oxygen and nutrients into the interior of the scaffold [19].

Thus, there are still two major shortcomings of bone grafts that need to be addressed: the initial host bone marrow absorption and the quality of nutrient flow into and out of the graft. To this end, we have proposed a scaffold with architecture specifically designed to enhance fluid absorption and retention. Our scaffold exhibits highly trabecular-like structures with intentionally engineered macro-pores, micro-channels, and nano-pores. The collective effect of these structures results in a synthetic construct that actively initiates bone marrow absorption and uniform distribution of bone marrow content. On the cellular level, the design of our scaffolds will induce exceptional cell attachment, proliferation, and differentiation on a uniform scale throughout the bone defect.

We have obtained *in vitro* data that indicates the previously stated properties. However, in order to develop a model explaining the theory behind our scaffold properties, we have created a Computer Aided Design (CAD) of the internal structures in our scaffolds.

## 2. Materials and methods

### 2.1. Fabrication of a three-leveled scaffold structure

In order to mimic the fluid/gas-conducting channels found in natural bones, we engineered micro-channels within the trabecular septa of our scaffolds. We used a polyurethane (PU) template (60 pores per inch (ppi): E.N. Murray Co., Denver, CO) and coated it with nano-sized hydroxyapatite (HA) powders (HA: OssGen Co., Gyeongsan, Korea) in a distilled water-based slurry. Because PU templates have a pre-defined porosity, we were able to adjust the size of the scaffold primary macro-pores, dimensions, and geometry by selecting PU templates of different pores per inch. To complete a homogeneous and continuous capillary structure, the fabrication steps were precisely controlled throughout the entire procedure. (1) The PU templates were pre-treated with 4% NaOH solution for 20 min in an ultra-sonicator to modify the surface property and then dried at 40 °C in an oven. (2) The 25 ml of coating solution mixed with 3 wt% polyvinyl alcohol (89,000–98,000 Mw, Sigma-Aldrich, USA), 1 wt% sodium carboxymethyl cellulose (ultra low viscosity, Sigma-Aldrich, USA), 3 wt% ammonium polyacrylate dispersant (Darvan 821, R.T. Vanderbilt, USA), and 2 wt% Glycerin (Sigma-Aldrich, USA) was prepared. The amount of the reagent was measured *versus* powder content, respectively. (3) 8 g of the HA nano-sized powder was slowly added to the coating solution while stirring and heating to condense until the powder/solution ratio reach to 1.77–1.80. (4) The treated PU template was immersed into the coating slurry and squeezed a couple times until the slurry coated the PU template homogenously. The amount of

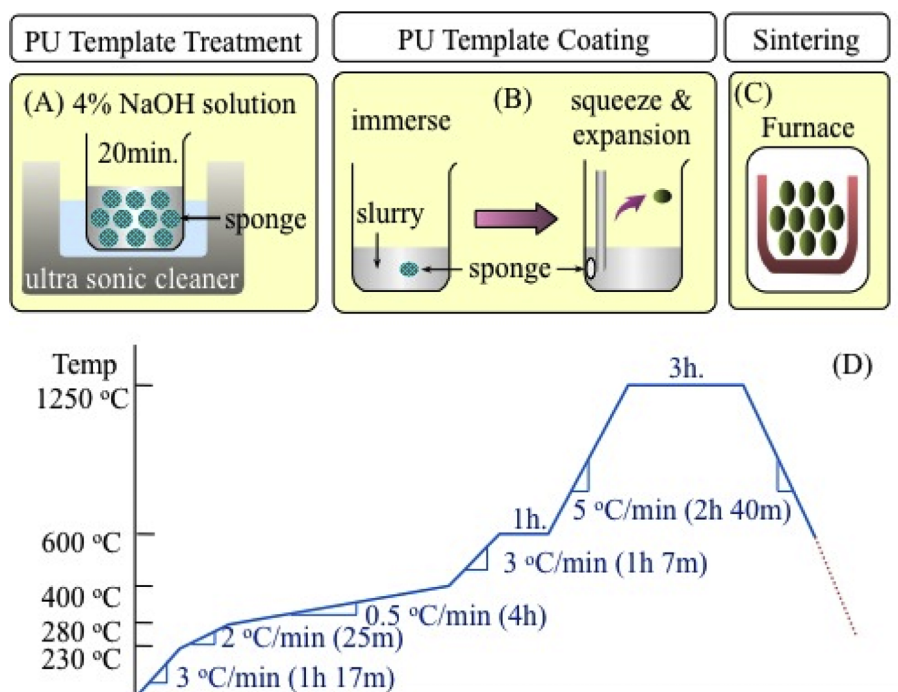


Fig. 1. MCNP scaffold fabrication procedures: (A) the treatment of PU template for surface modification, (B) the coating step of PU template with HA slurry, (C, D) the heat treatment of HA coated PU template using high temperature furnace.

slurry to coat one PU template was eight-fold of the template by weight. (5) The excess slurry was removed by using low air pressure. This also ensured the integrity of the macro-pores in the scaffold. (6) The coated template was dried overnight under cooling conditions (20–25 °C) with gentle air circulation. (7) Finally, the completely dried specimens were sintered according to 8-step heat treatment procedure in a high temperature furnace at 1250 °C for 3 h (Fig. 1). The PU template was incinerated during the sintering procedure, thus leaving behind a void we define as micro-channels. On the other hand, the HA slurry that had coated the PU template solidified to become dense trabecular septa.

## 2.2. Microstructural analysis

The microstructural characteristics of the MCNP scaffold such as 3D architecture, mechanical stability, pore size, porosity, and interconnectivity were characterized using SEM (Zeiss Supra 55VP, Carl Zeiss Inc), micro-CT (SkyScan 1172), mechanical testing (5848 Instron MicroTester), and helium pycnometry (porosity: AccuPyc II 1340 micromeritics). We had three scaffold groups based on their average macro-pore sizes (450  $\mu\text{m}$ , 320  $\mu\text{m}$ , and 200  $\mu\text{m}$ ) with each group having ten scaffolds.

In order to determine trabecular bone-like organization, traditional histomorphometric parameters were computed for each of the scaffolds over a 3D volume at the scaffold midsection that encompasses the axial cross-section of the

scaffold ( $n=5$ ). This area was 1.75 mm thick. A total of 4 cross sections were prepared from each scaffold and parameters were defined using traditional histomorphometry guidelines for trabecular bone structures as follows [20,21]:

- (a) % Scaffold volume [ $\text{SV}/\text{TV} = \text{scaffold volume}/\text{total volume} \times 100\%$ ].
- (b) Ratio of scaffold surface perimeter to total volume [ $\text{SS}/\text{TV} = \text{surface length}/\text{total volume}$ ].
- (c) Ratio of scaffold surface perimeter to scaffold volume [ $\text{SS}/\text{SV} = \text{surface length}/\text{scaffold volume}$ ].
- (d) Trabecular thickness [ $\text{Tb.th.} = (4/1.199) \times (\text{SS}/\text{SV})$ ].
- (e) Trabecular number [ $\text{Tb.n.} = ((4/\pi) \times (\text{SV}/\text{TV})) - 0.5/(\text{Tb.th.})$ ].
- (f) Trabecular separation [ $\text{Tb.sp.} = ((4/\pi) \times (\text{TV}/\text{BV}) - 1) \times (\text{Tb.th.})$ ].

We also measured the compression strength of cylindrical MCNP scaffolds with different macro-pore sizes (450  $\mu\text{m}$ , 320  $\mu\text{m}$ , and 200  $\mu\text{m}$ ) with each group containing 10 scaffolds. Each MCNP scaffold within a customized fixture was placed into an Instron 5848 MicroTester. A ramp was displaced at a rate of 0.125 mm/min to scaffold failure. The MCNP scaffolds were cylindrical with dimensions of 16 mm in height and 8 mm in diameter so that they would meet the 2:1 height to diameter ratio specified in the ASTM D695 compression testing standard.

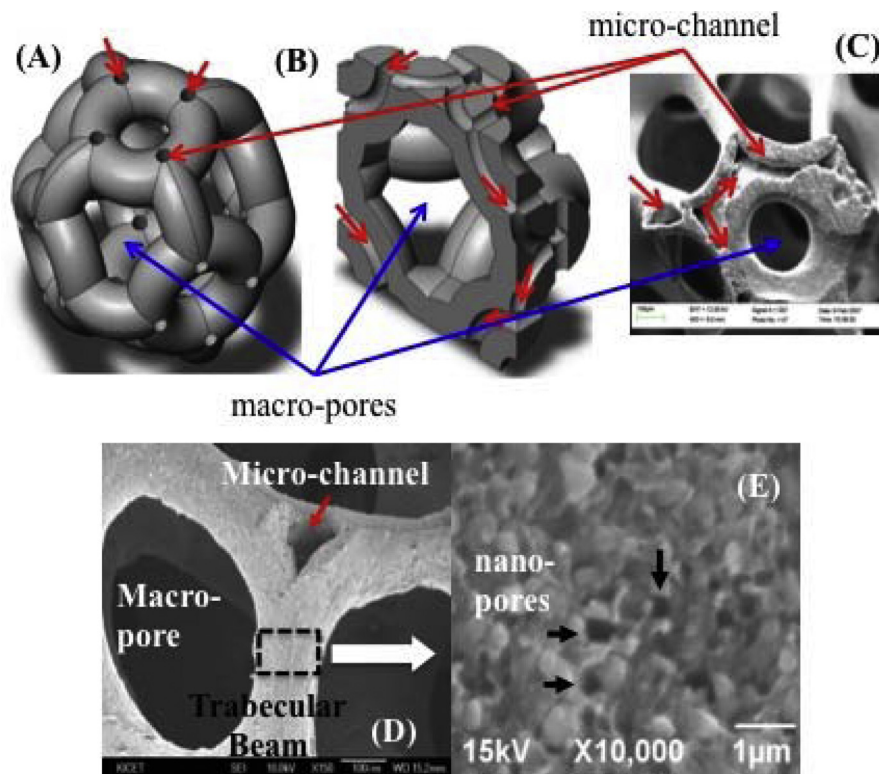


Fig. 2. Schema of trabecular bone composed of macro-pores and micro-channels (A) and cross section view (B) by CAD. SEM cross-section image of engineered micro-channel within trabecular septum of MCNP scaffold (C, D) and depiction of nano-pores (black arrow) on the surface of trabecular septum (E). Red arrows represent fluid flow through micro-channels for continuous supply of nutrients, gas, etc. (For interpretation of the references to color in this figure legend, the reader is referred to the web version of this article.)

### 2.3. Virtual representation of the surface area and porosity by Computer Aided Design (CAD) of micro-channels scaffold

A CAD model of our MCNP scaffolds was developed to investigate the effect micro-channels have on scaffold porosity and surface area per volumetric unit (Solidworks®, Dassault Systems Solidworks, MA, USA). We first developed a CAD model of a closed trabecular scaffold (without micro-channels) based on an open-unit truncated octahedron scaffold design then 50  $\mu\text{m}$  diameters of the channels inside the curved-rods were created along the axis of the six curved-rods [22,23]. This unit model was chosen to suitably represent the original 3D structure of the scaffold. This model was easy to create a periodic unit that could be spatially organized to maximize true scaffold volume. To calculate the surface area and porosity, the geometric parameters of the model were chosen as follows: 100  $\mu\text{m}$  diameter of the trabecular septum, 500  $\mu\text{m}$  height of the scaffold model unit, and 50  $\mu\text{m}$  diameters of the channels inside the trabecular septum (Fig. 2A and B). The porosity and the surface area of the scaffold units with and without micro-channels were measured using the functions of the solid and void volumes, and the surface area in the CAD software.

### 2.4. Bone marrow absorption and retention capabilities of MCNP scaffold

The absorption and retention capabilities of the MCNP scaffold were compared with those of decellularized human allografts (2 cm in height  $\times$  1 cm in width  $\times$  1 cm in depth cuboidal). The scaffold and allograft were placed vertically into 5 ml of bone marrow until the bone marrow stopped flowing to the top end of each respective structure. The absorption process (bone marrow rising to the top of the scaffold/allograft) and retention potential (ability to keep the bone marrow at that same height of absorption) were recorded and compared. We expected the micro-channels to be primarily responsible for capillary action, which we anticipated would also prime cells for homogenous spreading and settlement.

### 2.5. Preliminary mobilization and habitation of cells in vitro

In addition to ingress and retention, we also tested the characteristics of cell habitation in the MCNP scaffold. Thus, we examined efficiency of cell mobilization, adhesion, and migration *in vitro*. The osteoblastic MC3T3 cells were cultured in non-osteogenic media consisting of  $\alpha$ -MEM, supplemented with 10% Fetal Bovine Serum (FBS) (Gibco, USA) and 1% Antibiotics (streptomycin and penicillin) (Gibco, USA) at 37 °C in a humidified atmosphere containing 5% CO<sub>2</sub>. In order to simulate cell mobilization in challenging healing environments, we placed scaffolds vertically in the culture plates. Thus, any physical mobilization or migration would have been against gravity. If cells can be relocated against gravity, cell mobilization should not be compromised by any external forces *in vivo*.

*Cell culture in vertically oriented scaffolds:* 1.5 ml cell-suspensions at  $1 \times 10^6$  cell density were added to 24 well

plates. The 2 cm height cuboidal MCNP scaffolds (2 cm in height  $\times$  1 cm in width  $\times$  1 cm in cuboidal depth;  $n=5$ ) were vertically placed into the wells and allowed to absorb the cell suspensions for 5 min. Afterwards, 1.0 ml of non-osteogenic  $\alpha$ -MEM medium was added to each well. The media reached only half the height of the scaffolds from the bottom. After the media was added, we investigated cell hosting and vertical cell migration against gravity in the scaffolds. The efficacy of cell mobility was determined by measuring the height at which the cell front had reached. The heights were measured at time points of 24 h and 48 h with hematoxylin and eosin staining.

*Cell culture in horizontally oriented scaffolds:* Simultaneously, we investigated homogeneous cell ingress and habitation in 4 cm long cuboidal MCNP scaffolds (4 cm in height  $\times$  1 cm in width  $\times$  1 cm in cuboidal depth;  $n=5$ ). A 4 cm defect is clinically relevant as a critical size long bone defect. A 3.0 ml cell-suspension with a density of  $4 \times 10^6$  cells was added to each well in customized plates where the scaffolds were laid horizontally ( $n=5$ ). The scaffolds were allowed to absorb the cell suspensions for 5 min, and afterwards, 5.0 ml of non-osteogenic  $\alpha$ -MEM medium was added to the wells. The media completely covered the horizontally oriented scaffolds, allowing cells attached to any part of the scaffold to have access to surrounding media. We investigated cell migration and cell homing throughout the horizontally oriented scaffolds. The efficacy of cell attachment and mobility was measured after 48 h by hematoxylin and eosin staining.

### 2.6. Statistical analysis

All data were expressed as means  $\pm$  standard deviation (SD). Statistical differences were analyzed using one-way ANOVA, with Tukey's test used for post hoc comparison at a  $p < 0.05$  significance level.

## 3. Results

### 3.1. Microstructure analysis

#### 3.1.1. Micro-Computed Tomography (micro-CT) and mechanical strength

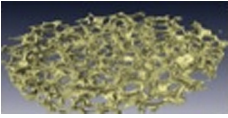
Morphometric analysis was carried out on CT images using a CT analyzer vs.1.4 (Skyscan). The histomorphometric parameters of the MCNP scaffolds were closely matched with human lumbar vertebrae trabecular bone (Table 1).

By measuring the area under the stress-strain curve, we calculated the strain energy density (compression strength) for each sample. MCNP scaffolds with average 320  $\mu\text{m}$  macropores exhibited  $82.2 \pm 3.48\%$  porosity and 3.2–4.3 MPa in compressive strength, which is comparable to that of human trabecular bones of 0.3 g/cc bone density (Fig. 3) [24]. By measuring the void volume fraction of the scaffold, we determined the porosity while the solid volume of the scaffold was measured using helium pycnometry. By subtracting the solid volume from the cylindrical volume, we calculated the void volume, which we quantified as porosity in terms of cubic units. We weighed the samples and used the specific gravity of



Table 1

Histomorphometry parameters of scaffold compared to those of human lumbar vertebrae trabecular bone ( $n=5$ ).

	MCNP scaffold	Lumbar vertebrae [21]
		
Bone volume/total Volume (%)	$16.06 \pm 2.8$	$10.3 \pm 2.0$
Bone surface/total Volume ( $\text{mm}^{-1}$ )	$7.6 \pm 0.7$	$9.5 \pm 1.6$
Bone surface/bone Volume ( $\text{mm}^{-1}$ )	$33.9 \pm 6.3$	$25.9 \pm 1.7$
Trabecular number ( $\text{mm}^{-1}$ )	$1.59 \pm 0.2$	$1.47 \pm 0.4$
Trabecular separation ( $\mu\text{m}$ )	$526.1 \pm 80.9$	–
Trabecular thickness ( $\mu\text{m}$ )	$100.8 \pm 11.6$	$103.2 \pm 10.3$

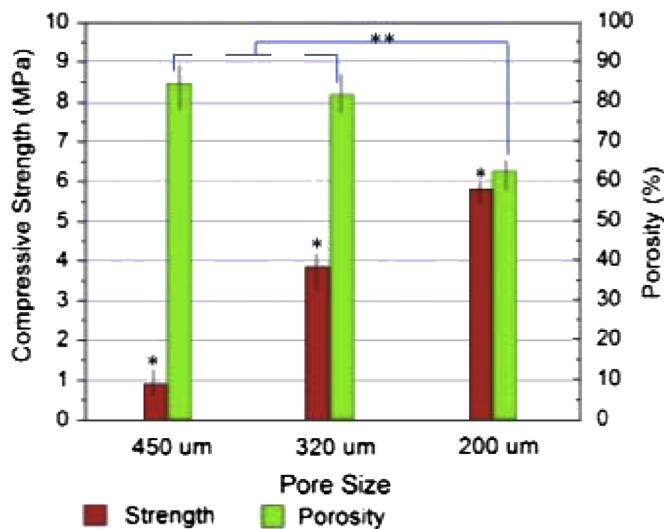


Fig. 3. The compressive strength for three different pore sizes showing significant increase among groups (\*) with both 450  $\mu\text{m}$  and 320  $\mu\text{m}$  scaffolds showing higher porosity than 200  $\mu\text{m}$  scaffolds (\*\*). ( $n=10$ ,  $p < 0.05$ ).

hydroxyapatite as a control to check the accuracy of the pycnometry measurements. The MCNP scaffold with 450  $\mu\text{m}$  and 320  $\mu\text{m}$  diameter macro-pores demonstrated similar porosity with that of normal human bone (Fig. 3) [25].

### 3.1.2. Computer Aided Design (CAD) and Scanning Electron Microscopy (SEM)

To enhance cell mobilization, fluid access, and gas exchange we developed interconnected micro-channels and nano-pores in our scaffold. Based on the calculations using CAD, the surface area was significantly higher (+41.96%) in scaffolds with micro-channels present as opposed to scaffolds without them. At the same time, the overall porosity did not change significantly (+8.8%) (Figs. 2A, B and Table 2). The CAD model illustrates macro-pores (blue arrows) and micro-channels within each trabecular septum (red arrows). These details in the CAD scheme are clearly detected in SEM images of our scaffolds (Fig. 2C). As opposed to the CAD model, there are visible cracks in the scaffold that may compromise the mechanical strength. However, in our scaffolds we created crack-free scaffolds by precisely controlling the Fion procedure (Fig. 1). As shown in Figs. 4(B) and (C), the coated, dried, and sintered scaffolds were smooth

Table 2

The comparison of porosity and surface area of scaffolds with and without micro-channels using CAD.

	Porosity (%)	Macro-pore ( $\mu\text{m}$ )	Trabecular beam ( $\mu\text{m}$ )	Micro-channel ( $\mu\text{m}$ )	Surface area
Non-channel	79.5	300	100	None	8.307 $\text{mm}^2$
With-channel	86.5	300	100	50	11.793 $\text{mm}^2$
	+8.8			++++	+41.96%

without cracks. The overall structure of the MCNP scaffold was similar to those of human trabecular bone (Fig. 4C and D). Each trabecular septum had micro-channels that established additional accesses for body fluid and gas exchange (Figs. 2C and D). In addition, each trabecular septum had nano-sized pores on its surface (Fig. 2E). In order to compensate for the absence of cells, blood circulation and lymphatic channels of artificial scaffolds, these micro-channels will be created for super-efficient mobilization of host cells, bone marrow, and blood at the repair sites.

Moreover, SEM images showed (1) fully interconnected macro-pores (300–400  $\mu\text{m}$ ) trabecular structures, (2) intra-septal micro-channels (25–70  $\mu\text{m}$ ), and (3) trabecular beams (85–120  $\mu\text{m}$ ) with nano-pores (100–400 nm) on the trabecular surface (Figs. 2 and 4). These three components are intended to provide human trabecular bone networks, body fluid access, diffusion, nutritional supply, gas exchange, communication around the bone, and cell anchorage.

### 3.2. Bone marrow absorption and retention capability of the MCNP scaffold

Scaffolds do not have intricate networks of blood vessels and bone marrow. It is essential for any scaffold to absorb bone marrow, which contains many growth factors essential for bone repair. Our data showed exceptional absorption and retention of cells throughout the entire 2 cm long scaffolds. Thus, we further examined the absorption and retention capability of the MCNP scaffold with bone marrow. The MCNP scaffolds demonstrated higher bone marrow ingress than the decellularized cadaveric human bones of the same size and shape. The bone marrow front reached the top of the MCNP scaffold (2 cm in height) after 12 s while the bone marrow front only reached 1.5 cm of the allograft's height (2 cm in height) after 120 s (Fig. 5). The saturation potential against gravity for the MCNP scaffold was 100% whereas in the allograft, it was only 75%.

### 3.3. Preliminary mobilization and habitation of cells in vitro

We examined the ingress and habitation capability of the MCNP scaffolds via the collective internal structures (macro-pores, micro-channels, and nano-pores) using MC3T3 cells.

**Cell culture in vertically oriented scaffolds:** We put 1.5 ml cell suspension of  $1 \times 10^6$  cells into a 24 well plate on which we placed 2 cm in height cuboidal MCNP scaffolds. Within

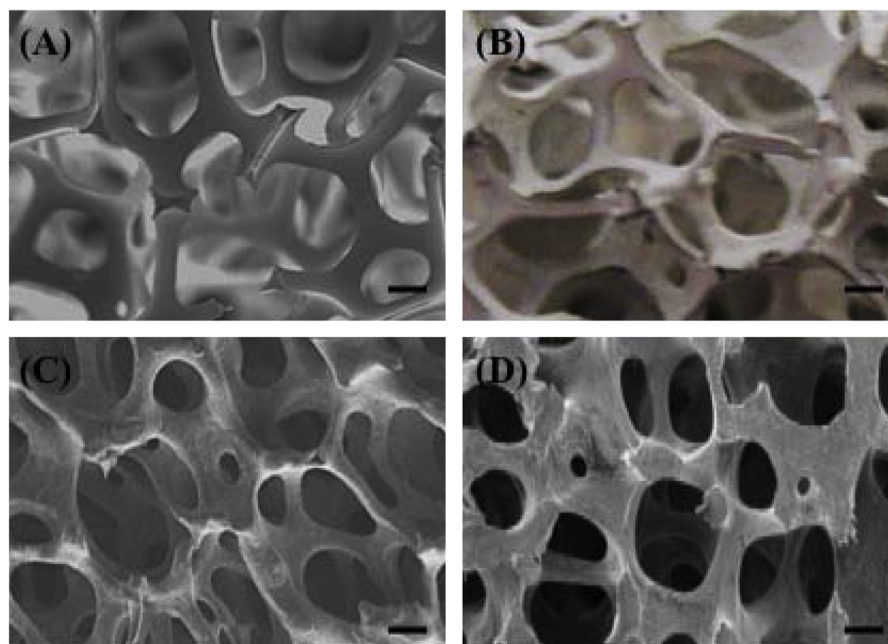


Fig. 4. SEM and digital images of PU template (60 ppi) and MCNP scaffold: (A) PU template (SEM), (B) after coating and drying (digital), (C) after sintering (SEM), and (D) human lumbar vertebrae trabecular bone (SEM). (Scale bar = 200  $\mu$ m).

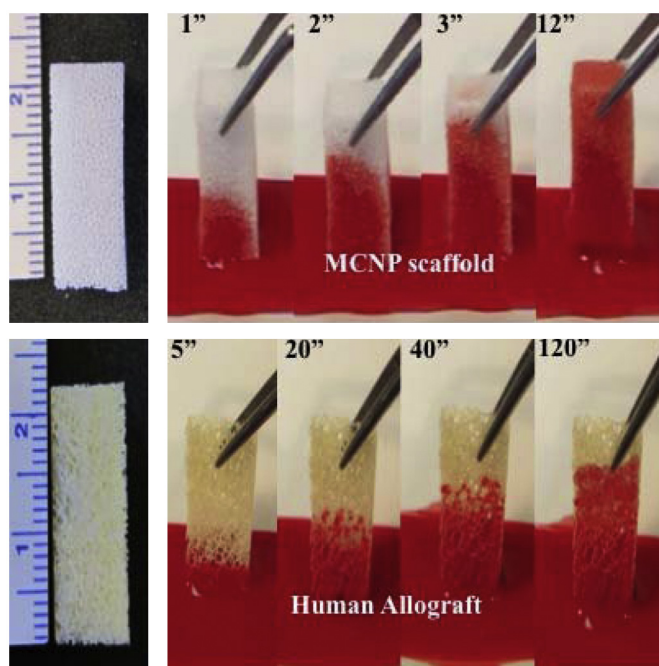


Fig. 5. Comparison of the 'Absorption Property' using bone marrow: MCNP scaffold demonstrated 10 times faster ingress than decellularized human allograft ( $1 \times 1 \times 2.2$  cm).

seconds, the scaffold absorbed the entire cell suspension. After 5 min we added 1.0 ml of media so that the media filled the well up to height at which the midpoint of the scaffold stood. The top of the media line separated the upper half of the scaffold (exposed to air) which relied on fluid and gas exchange from the bottom half. After time point of 24 and 48 h, the cell front reached approximately  $83 \pm 3\%$  and

$90 \pm 5\%$  of the total scaffold height, respectively (H&E stain) (Fig. 6).

*Cell culture in horizontally oriented scaffolds:* Similar to the vertically oriented 2 cm in height scaffolds, the 4 cm in length scaffold which was horizontally oriented in the culture plate exhibited effective ingress and habitation after 48 h as well. Microscopic examination showed even distribution, settlement, and networking of mobilized cells (Fig. 7). In addition, inside the scaffold, the cells synthesized a matrix on the scaffold surface and began to crosslink from one side of a macro-pore to the other side. Most importantly, we confirmed the presence of cells in the micro-channels. This suggests that the micro-channels not only enhance fluid ingress but also provide additional space for cell habitation (Fig. 8).

The combined effects of the macro-pores, micro-channels, and nano-pores result in a construct that enhances bone marrow ingress and uniformly distributed cell populations throughout the entire scaffold.

#### 4. Discussion

The ultimate goal of creating a scaffold for bone is to fully regenerate bone from one host-graft junction to the other host-graft junction. Many leading investigators demonstrated exciting results of successful bone regeneration using scaffolds, pre-loaded cells and growth factors [4–6]. However, in order to accomplish fully bone regeneration, there needs to be a time-dependent influx of host bone marrow into the defect in order to ensure uniformly distributed cell attachment as well as a high volume of gas and nutrient exchange at all parts of the defect. In effect, the scaffold must actively initiate and facilitate the bone healing instead of merely existing as a passive synthetic template. There are various types of scaffolds made of polymers, ceramics,

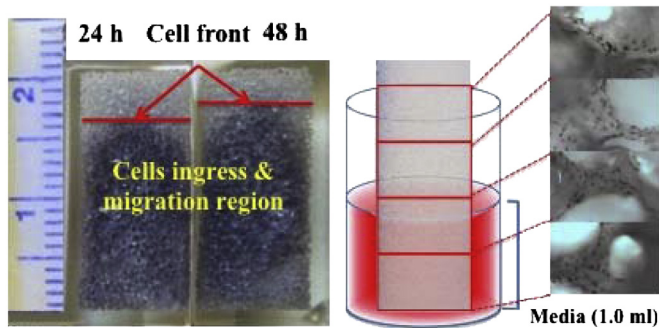


Fig. 6. Cell ingress and migration into MCNP scaffold ( $1 \times 1 \times 2$  cm height) after 24 and 48 h at cell density of  $1 \times 10^6$  (left). The 1.5 ml cell suspension was added into a 24 well plate. Then the scaffold was placed into the culture plate for 5 min to absorb the entire cell suspension; 1.0 ml non-osteogenic media was then added into well (right, H&E stain).

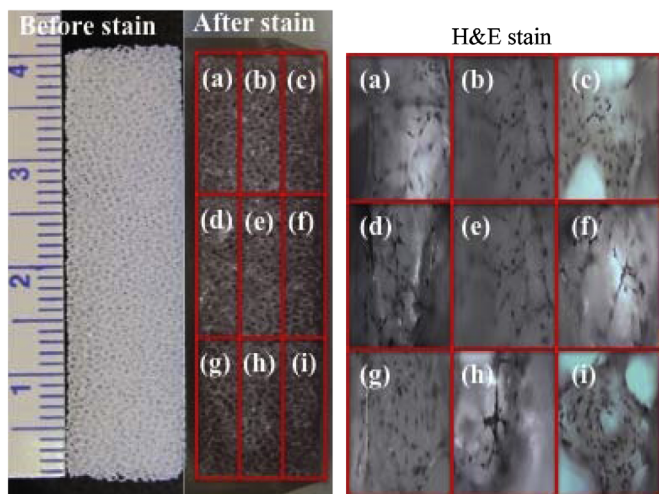


Fig. 7. Homogeneous cell ingress and attachment through entire MCNP scaffold ( $1 \times 1 \times 4$  cm long) after 48 h at cell density of  $4 \times 10^6$  with non-osteogenic media. The picture of the scaffold on the left was taken before staining and the pictures of the scaffold cross-sections on the right were taken after H&E staining.

trabecular metals, and composite material; but materials themselves do not necessarily address the initial cell ingress or nutrient flow. The materials mostly contribute to the mechanical strength and compatibility of cells only after they have infiltrated the scaffold. However, as we have stated before, the absorption power of the scaffold is an aspect of bone healing that has not necessarily been directly addressed. Furthermore, HA is known for its biocompatibility and osteoconductive capacities [26]. Compared with other bone substitutes (e.g. collagen scaffolds), HA is characterized by its precisely defined physical and chemocrystalline properties, high level of purity, and uniformity of chemical composition so that its biological reactions can be fairly predicted. HA can be used to fabricate highly porous scaffolds with good structure continuity, which may ensure intercellular communication among osteogenic cells resting on the HA surface

[27]. To this end, we have developed a hydroxyapatite-based scaffold, which exhibits superior fluid absorption power and retention capacity that effectively draws in bone marrow and stimulates natural bone repair.

The method of scaffold fabrication used in this study is the PU template coating method. It enables the scientist to create scaffolds with interconnected pores while being able to control the sizes of the primary macro-pores, micro-channels, and nano-pores. The PU template coating method is versatile (i) to prepare well-controlled macro-porous structures, which depend on the pre-defined template structures (*i.e.* 60 pores per inch template; 300–400  $\mu\text{m}$  pore diameter) most optimized pore size for osteoblast differentiation, (ii) to construct continuous micro-channels. Moreover, there are no limitations in terms of creating customized shapes for the scaffold since the PU template can be cut into any desired shape (Fig. 9).

As discussed in many leading investigations, the major disadvantage of utilizing the polymer foam method is the weak mechanical strength due to the formation of cracks. In this study, as described in 2.1 and 3.1.2, the conditions from the amount of slurry to the drying and sintering conditions were precisely controlled to maintain a crack-free structure. Although the engineered MCNP scaffolds demonstrated relatively acceptable compressive strength (3.2–4.3 MPa), we believe that the mechanical strength of the regenerated bone will exhibit even more compressive strength than bone regenerated from scaffolds that do not address bone marrow ingress and nutrient flow.

In this study, the MCNP scaffolds demonstrated higher bone marrow ingress than decellularized human cadaveric bones of the same size and shape. Furthermore, the initial mobilization and retention of cell-containing solution by the MCNP scaffolds led to homogenous cell spreading, attachment, growth, and matrix formation against gravity. The reason for this superior ingress phenomenon can be supported by the macro-pores and micro-channels in the scaffold. As shown in Fig. 5, the fast ingress of bone marrow in the scaffold exhibited a higher rate of work done than in the allografts. We can assume that there is some sort of work done because the direction of absorption was against gravity. From this we derived that the power of absorption equals work done (capillary action against gravity  $\times$  distance) over time. Thus, as it takes longer for a structure to absorb bone marrow, there is less power and may result in less total bone marrow absorbed. And as our data shows, the allograft was not saturated 100% whereas the MCNP scaffold was in a very short period of time.

The initial ingress and retention of cell-containing bone marrow by the MCNP scaffold led to cell dispersion, attachment, growth and matrix formation, all in homogenous fashion. This means that the MCNP scaffold is readily capable of promoting natural bone healing through ingress of adjacent osteogenic and angiogenic progenitor cells at the wound healing site with less dependence on pre-loaded cells. In addition to the transport and attachment of cells into the scaffold against gravity, the cells even at the top of the cell front exhibited healthy morphology and matrix formation. As shown in Figs. 7 and 8, the saturated MCNP scaffold



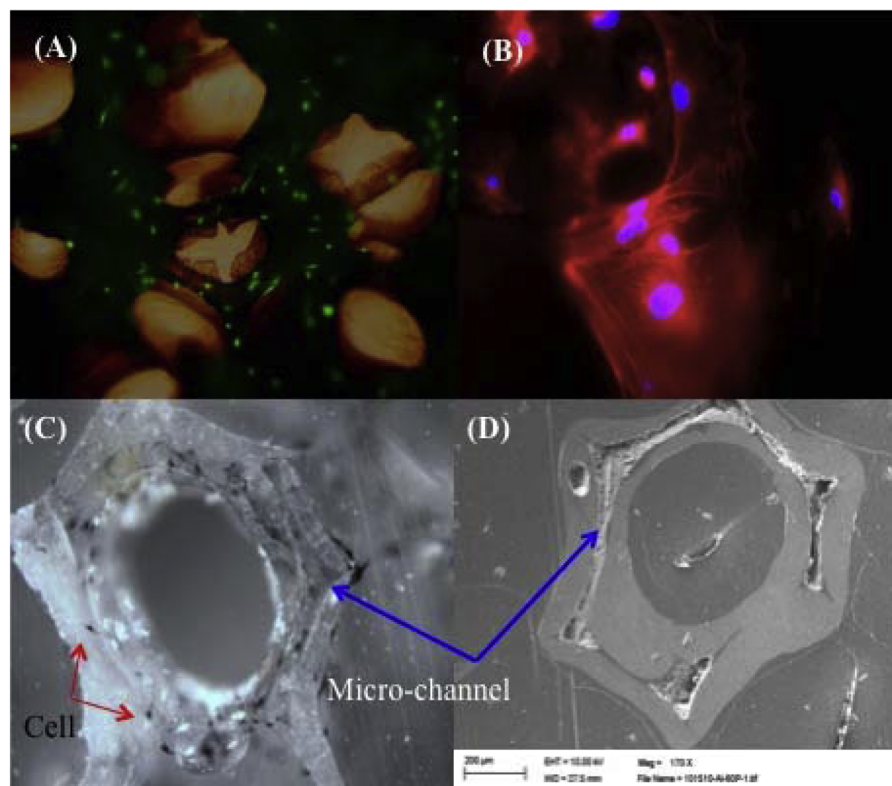


Fig. 8. The migration and attachment of MC3T3 cells on the MCNP scaffold surface and micro-channels: (A) fluorescence image of calcein labeled  $20\times$ , (B) fluorescence image showed cell nuclei (blue) and actin filaments (red)  $100\times$ , (C) infiltration and migration into micro-channels  $40\times$ , and (D) SEM of micro-channels. (For interpretation of the references to color in this figure legend, the reader is referred to the web version of this article.)



Fig. 9. Scaffold of finger using PU template coating method by HA slurry.

provided a microenvironment dynamic enough for cells to mobilize, attach, and proliferate. We believe that fluid ingress *in vivo* will be even more effective since the MCNP scaffold will have both proximal and distal access to bone marrow as opposed to one cell suspension at the bottom of the culture plate.

This biologically dynamic HA scaffold offers several advantages. In addition to the interconnected macro-pores (300–400  $\mu\text{m}$ ) that mimic human trabecular bone, these scaffolds contain micro-channels (25–70  $\mu\text{m}$ ) within each trabecular septum. By simulating innate structures found in bone, we aimed to create an active bone template that exhibited a

dynamic environment in terms of nutritional supply, gas exchange, cell communication, and potential mechanosensory mechanisms induced by fluidic forces. By nature, channels with diameters on the micron scale exhibit highly effective fluid absorption, and we expected them to be primarily responsible for capillary action. We also believe that because capillary action can exert a fluidic force on attached cells, the presence of micro-channels may induce a mechanically induced mechanism for cell proliferation or differentiation. Because this study documented the concept of distinct bone marrow absorption and retention, further studies on capillary action quantification will be done. Another element that enhances the biological environment of our scaffolds is the nano-pores (100–400 nm) on the surface of the trabecular septa. Since cells have been documented to be sensitive to nano-patterns [28,29], we expect that these nano-pores play a role in increasing cell attachment.

These approaches address the major barrier of insufficient bone marrow infiltration into synthetic constructs and the inability to regenerate bone in large defects on scale of several centimeters. To confirm more relevant cell responses such as osteogenic differentiation, matrix formation, and mineralization, further *in vitro* studies will need to mimic conditions in the bone where fluidics and piezoelectricity are major factors.

Based on our promising data, we may consider that the absorption and retention properties of the MCNP scaffold will promote ingress of adjacent osteogenic and angiogenic



progenitor cells at the site of the defect with less dependence on pre-loaded cells and growth factors. We will have to further address these properties *in vivo* in future studies.

## 5. Conclusion

A hydroxyapatite scaffold with micro-channels and nano-pores (MCNP) was successfully developed using a polyurethane template coating method to utilize in tissue engineering. The fluid absorption and retention capabilities of these scaffolds were highly efficient in bone marrow ingress and induction of cell proliferation. These characteristics were tested with a 2 cm height scaffold vertically oriented on a culture plate; another test was done with a 4 cm length scaffold horizontally oriented on a culture plate. The cells attached and proliferated on both vertical and horizontal scaffold studies. In the vertically oriented 2 cm scaffold, the cell front reached  $83 \pm 3\%$  and  $90 \pm 5\%$  of the 2 cm height at 24 h and 48 h respectively. In the horizontally oriented 4 cm scaffold, the entire scaffold was covered in cells within 48 h. In both scaffold groups, the cells remarkably produced ECM on the scaffold surface as well as in the macro-pores. We also confirmed the presence of cells in the micro-channels, suggesting that these channels not only enhance fluid ingress but may also provide additional space for cell habitation. The optimum mechanical strength ( $3.2\text{--}4.3$  MPa) and porosity ( $82.2 \pm 3.48\%$ ) were calculated on scaffolds with macro-pores of 320  $\mu\text{m}$  in average diameter.

## Acknowledgment

This work was partially supported by National Agenda Project (NAP) funded by Korea Research Council of Fundamental Science & Technology (P-09-JC-LU63-C01).

## References

- [1] V. Karageorgiou, D. Kaplan, Porosity of 3D biomaterial scaffolds and osteogenesis, *Biomaterials* 26 (2005) 5474–5491.
- [2] A. Vats, N.S. Tolley, J.M. Polak, J.E. Gough, Scaffolds and biomaterials for tissue engineering: a review of clinical applications, *Clinical Otolaryngology* 28 (2003) 165–172.
- [3] D.W. Hutmacher, Scaffolds in tissue engineering bone and cartilage, *Biomaterials* 21 (2000) 2529–2543.
- [4] T.L. Arinzeh, T. Tran, J. Mcalary, G. Daculsi, A comparative study of biphasic calcium phosphate ceramics for human mesenchymal stem-cell-induced bone formation, *Biomaterials* 26 (2005) 3631–3638.
- [5] X.H. Zou, H.X. Cai, Z. Yin, X. Chen, Y.Z. Jiang, H. Hu, et al., A novel strategy incorporated the power of mesenchymal stem cells to allografts for segmental bone tissue engineering, *Cell Transplant* 18 (2009) 433–441.
- [6] I. Ono, T. Yamashita, H.Y. Jin, Y. Ito, H. Hamada, Y. Akasaka, et al., Combination of porous hydroxyapatite and cationic liposomes as a vector for BMP-2 gene therapy, *Biomaterials* 25 (2004) 4709–4718.
- [7] J.R. Woodard, A.J. Hillmore, S.K. Lan, C.J. Park, A.W. Morgan, J.A. Eurell, et al., The mechanical properties and osteoconductivity of hydroxyapatite bone scaffolds with multi-scale porosity, *Biomaterials* 28 (2007) 45–54.
- [8] I. Manjubala, A. Woesz, C. Pilz, M. Rumpler, N. Fratzl-Zelman, P. Roschger, et al., Biomimetic mineral-organic composite scaffolds with controlled internal architecture, *Journal of Materials Science: Materials in Medicine* 16 (2005) 1111–1119.
- [9] R.E. Unger, A. Sartoris, K. Peters, A. Motta, C. Migliaresi, M. Kunkel, et al., Tissue-like self-assembly in cocultures of endothelial cells and osteoblasts and the formation of microcapillary like structures on three-dimensional porous biomaterials, *Biomaterials* 28 (2007) 3965–3976.
- [10] A.S. Goldstein, T.M. Juarez, C.D. Helmke, M.C. Gustin, A.G. Mikos, Effect of convection on osteoblastic cell growth and function in biodegradable polymer foam scaffolds, *Biomaterials* 22 (2000) 1279–1288.
- [11] S. Hofmann, H. Hagenmüller, A.M. Koch, R. Müller, G. Vunjak-Novakovic, D.L. Kaplan, et al., Control of *in vitro* tissue-engineered bone-like structures using human mesenchymal stem cells and porous silk scaffolds, *Biomaterials* 28 (2007) 1152–1162.
- [12] O. Gauthier, J.M. Boulter, E. Aguado, P. Pilet, G. Daculsi, Macroporous biphasic calcium phosphate ceramics: influence of macropore diameter and macroporosity percentage on bone ingrowth, *Biomaterials* 19 (1998) 133–139.
- [13] A. Bignon, J. Chouteau, J. Chevalier, G. Fantozzi, J.P. Carret, P. Chavassieux, et al., Effect of micro- and macro-porosity of bone substitutes on their mechanical properties and cellular response, *Journal of Materials Science: Materials in Medicine* 14 (2003) 1089–1097.
- [14] L.M. Mathieu, T.L. Mueller, P.E. Bourban, D.P. Pioletti, R. Müller, J.A. Manson, Architecture and properties of anisotropic polymer composite scaffolds for bone tissue engineering, *Biomaterials* 27 (2006) 905–916.
- [15] Y.W. Wang, Q. Wu, J. Chen, G.Q. Chen, Evaluation of three-dimensional scaffolds made of blends of hydroxyapatite and poly-(3-hydroxybutyrate-co-3-hydroxyhexanoate) for bone reconstruction, *Biomaterials* 26 (2005) 899–904.
- [16] S.S. Kim, M. Sun Park, O. Jeon, C. Yong Choi, B.S. Kim, Poly(lactide-co-glycolide)/hydroxyapatite composite scaffolds for bone tissue engineering, *Biomaterials* 27 (2006) 1399–1409.
- [17] S.L. Ishaug-Riley, G.M. Crane, A. Gurlek, M.J. Miller, A.W. Yasko, M.J. Yaszemski, et al., Ectopic bone formation by marrow stromal osteoblast transplantation using poly(DL lactic-co-glycolic acid) foams implanted into the rat mesentery, *Journal of Biomedical Materials Research* 36 (1997) 1–8.
- [18] G. Vunjak-Novakovic, L.E. Freed, Culture of organized cell communities, *Advanced Drug Delivery Reviews* 33 (1998) 15–30.
- [19] E. Sachlos, J.T. Czernuszka, Making tissue engineering scaffolds work. Review: the application of solid freeform fabrication technology to the production of tissue engineering scaffolds, *European Cells a Materials Journal* 5 (2003) 29–40.
- [20] L.P. Nogueira, D. Braz, R.C. Barroso, L.F. Oliveira, C.J. Pinheiro, D. Dreossi, et al., 3D histomorphometric quantification of trabecular bones by computed microtomography using synchrotron radiation, *Micron* 41 (2010) 990–996.
- [21] T. Sone, T. Tamada, Y. Jo, H. Miyoshi, M. Fukunaga, Analysis of three-dimensional microarchitecture and degree of mineralization in bone metastases from prostate cancer using synchrotron microcomputed tomography, *Bone* 35 (2004) 432–438.
- [22] N. Chantarapanich, P. Puttawibul, S. Sucharitpawatskul, P. Jeamwathanachai, S. Inglam, K. Sithiseripatip, Scaffold library for tissue engineering: a geometric evaluation, *Computational and Mathematical Methods in Medicine* 407805 (2012) 1–14.
- [23] L.J. Gibson, Biomechanics of cellular solids, *Journal of Biomechanics* 38 (2005) 377–399.
- [24] S.A. Goldstein, The mechanical properties of trabecular bone: dependence on anatomic location and function, *Journal of Biomechanics* 20 (1987) 1955–1961.
- [25] E. Tsuruga, H. Takita, H. Itoh, Y. Wakisaka, Y. Kuboki, Pore size of porous hydroxyapatite as the cell-substratum controls BMP-induced osteogenesis, *Journal of Biomechanics* 121 (1997) 317–324.
- [26] H. Yuan, K. Kurashina, J.D. de Bruijn, Y. Li, K. de Groot, X. Zhang, A preliminary study on osteoinduction of two kinds of calcium phosphate ceramics, *Biomaterials* 20 (1999) 1799–1806.

- [27] I.H. Jo, K.H. Shin, Y.M. Soon, Y.H. Koh, J.H. Lee, H.E. Kim, Highly porous hydroxyapatite scaffolds with elongated pores using stretched polymeric sponges as novel template, *Materials Letters* 63 (2009) 1702–1704.
- [28] Y. Wan, Y. Wang, Z. Liu, X. Qu, B. Han, J. Bei, et al., Adhesion and proliferation of OCT-1 osteoblast-like cells on micro- and nano-scale topography structured poly(l-lactide), *Biomaterials* 26 (2005) 4453–4459.
- [29] L. Zhao, S. Mei, P.K. Chu, Y. Zhang, Z. Wu, The influence of hierarchical hybrid micro/nano-textured titanium surface with titania nanotubes on osteoblast functions, *Biomaterials* 31 (2010) 5072–5082.